Proceedings of the
44th IEEE Conference on Decision and Control, and
the European Control Conference 2005
Seville, Spain, December 12-15, 2005

**ThB08.4**

# Parameter space PID design based on simulation and its application

Masami Saeki*

Department of Mechanical System Engineering

Hiroshima University

Higashi-Hiroshima 739-8527, Japan

saeki@hiroshima-u.ac.jp

Akihisa Takahashi**

Omron Healthcare Co., Ltd

Ukyo-ku, Kyoto 615-0084, Japan

*Abstract*— The parameter space PID design method based on the concept of unfalsified control is a data-driven model-free design method, and some set of PID gains that do not satisfy the mixed sensitivity performance index can be drawn on the PI or PD gain plane from the input output data directly. In this paper, this method is used for a simulation-based controller design and it is demonstrated by the design of a steering torque control. This method can be applied to any model, when the plant response data are available to a hundred of sinusoidal inputs by simulation.

Fig. 1.   Mixed sensitivity problem

## I. INTRODUCTION

Recently, more experiments have been replaced with simulation studies. Since the simulation model is usually nonlinear and high-dimensional, model-based controller design methods cannot be applied to such a complex model and a simplified model is constructed for controller design. In this situation, we consider that a controller design method that can be directly applied to the simulation model is useful.

The set of input output data is considered as a direct representation of the plant model [1], and if there exists a design method that is based on the input output data without any assumptions on the plant, the method will be applied to any plants. Unfalsified control concept gives a basic idea to realize such a method [2], and it has been applied to adaptive control[3], [4], [5] and off-line controller design[6], [7]. We have proposed a parameter space design method of PID controllers based on this concept [8].

Our method can be directly applied to the simulation-based design. However, success of the unfalsification method depends on the falsification efficiency, which deeply relates to the input-output data, but the relation was not examined sufficiently. Therefore, we have studied the relation by applying our method to a few numerical examples in [8] and [9], and we found that the PID gains are usually falsified effectively by our method if the plant responses to the sinusoidal inputs with many frequencies are used.

Of course, if the plant response is available by simulation, another method such as genetic algorithm can be applied to the minimization problem of the performance index. Compared with such a heuristic global optimization method, our parameter space design method has the following features. 1) The solution is given as a region of unfalsified gains on the parameter plane. The region gives us global information, which is useful for tuning. Also, it is useful for determining the proper search area of the PID gains for other methods
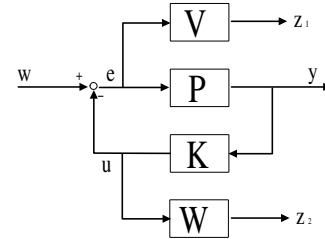
such as the genetic algorithm. 2) If all the PID gains are falsified, it is guaranteed that the problem is infeasible. 3) The region can be drawn very quickly if the response data are given. Therefore, most computational time is used for simulation.

In this paper, first, we will summarize the parameter space design method with some notes on the selection of input output data, and next we will apply it to a steering torque control problem.

## II. DESIGN METHOD

### A. Mixed sensitivity control problem

Let us consider a single input single output feedback system:

$$y = Pe \ , \ u = Ky \ , \ e = w - u \qquad (1)$$

where $y$, $u$, $e$, $w$ are discrete time signals with the sampling period $\Delta T$. $P$ is a plant and $K$ is a discrete time PID controller given by

$$K(z) = K_P + K_I \Delta T \frac{1}{z-1} + K_D h_D(z) \qquad (2)$$

where $h_D(z)$ is given by discretizing the approximate derivative element $s/(\tau s + 1)$ with the sampling period $\Delta T$. For this system, consider a mixed sensitivity control problem as shown in Fig. 1. Note that $P$ can be a nonlinear plant. The discrete time transfer functions $V(z)$ and $W(z)$ are assumed to be stable, and $z_1 = Ve, z_2 = WKy$. Then, the performance index is given by the $l_2$ gain condition:

$$\|z\|_2 < \gamma \|w\|_2, \quad w \in l_2 \qquad (3)$$

where $z = (z_1, z_2)^T$ and $\| \ \|_2$ denotes $l_2$ norm. Our problem is to draw the set of PID gains $(K_P, K_I, K_D)$ that do not satisfy the $l_2$ gain condition on the PI or PD planes.

Note that we do not obtain PID gains that satisfy the performance index but we try to obtain the gains that do not satisfy it. This guarantees that the unfalsified set does not become null if the problem has a solution.

### B. Falsification condition

First, calculate $y_I, y_D$ from the output data $y$ following

$$y_I = \Delta T \frac{1}{z-1} y \quad , \quad y_D = h_D(z) y \tag{4}$$

Then, calculate $y_W, y_{WI}, y_{WD}$ which are the responses of the weighting function $W(z)$ for the input signals $y, y_I, y_D$, respectively.

$$y_W = Wy \quad , \quad y_{WI} = Wy_I \quad , \quad y_{WD} = Wy_D \tag{5}$$

Set the column vectors $v_1, v_2$ as follows.

$$v_1(i) = [y_W(i), y_{WI}(i), y_{WD}(i)]^T \tag{6}$$
$$v_2(i) = [y(i), y_I(i), y_D(i), e(i)]^T \tag{7}$$

And also define the following matrices $c_1 \in R$, $R \in R^{3\times 3}$, $Q \in R^{3\times 3}$, $q \in R^{3\times 1}$, $c_2 \in R$.

$$c_1(m): = \sum_{i=1}^{m} z_1^2(i) \tag{8}$$

$$R(m): = \sum_{i=1}^{m} v_1(i)v_1(i)^T \tag{9}$$

$$\begin{pmatrix} Q(m) & q(m) \\ q^T(m) & c_2(m) \end{pmatrix} : = \sum_{i=1}^{m} v_2(i)v_2(i)^T \tag{10}$$

**Theorem 1 [8]**  *$l_2$ gain condition (3) is satisfied, only if*

$$p^T[Q(m) - \frac{1}{\gamma^2} R(m)]p + 2p^T q(m) + c_2(m)$$
$$- \frac{1}{\gamma^2} c_1(m) > 0, m = 1, 2, \ldots, M \tag{11}$$

*is satisfied for all $w \in l_{2e}$ where $M$ is the data length and $p = (K_P, K_I, K_D)^T$.*

**Remark 1**  Suppose that the data $e(m)$ and $y(m)$ are given for $m = 1, 2, \ldots, M$, then Theorem 1 gives $M$ falsification conditions. If we check all the conditions, it will take much computational time. When we use many sinusoidal responses, it is enough to check the condition (11) just for $m = M$ from our experience.

**Remark 2**  The coefficient matrices $Q(m)$, $R(m)$, $q(m)$, $c_2(m)$ are determined by $y(i)$, $e(i)$ for $i = 1, 2, \ldots, m$. The inequality is quadratic with respect to the parameter vector $p$, and the permissible region of (11) can be drawn for each $m$ on the parameter plane as follows. Namely, first, fix one of the PID gains, say $K_D = a$, and then rewrite (11) in the next form.

$$\tilde{p}^T \tilde{Q}(m)\tilde{p} + 2\tilde{p}^T \tilde{q}(m) + \tilde{c}(m) > 0 \tag{12}$$

where $\tilde{p}$ is a 2-dimesional vector consisting of the gains, say $\tilde{p} = (K_P, K_I)^T$, and the region can be drawn on the plane by applying the algorithm of [8]. The boundary of the falsified region is ellipse or hyperbola.

**Remark 3 Choice of** $w(t)$  The data $e(t)$ and $y(t)$ are calculated by simulating the feedback system for a reference input $w(t)$. Sinusoidal functions for about a hundred of frequencies are recommended for $w(t)$. However, things are not so simple, and note that the phase shifted sinusoidal function gives a sharper result than $w(t) = \sin \omega t$.

We will show this for a continuous time example where

$$P(s) = \frac{1}{s^2 + s + 1}$$
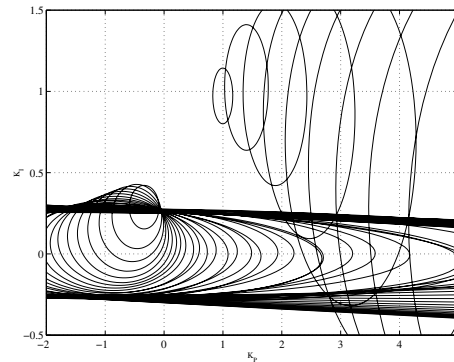$$V(s) = \frac{1.5s + 1}{3s + 0.02} , W(s) = 0$$

and we will clarify the reason.



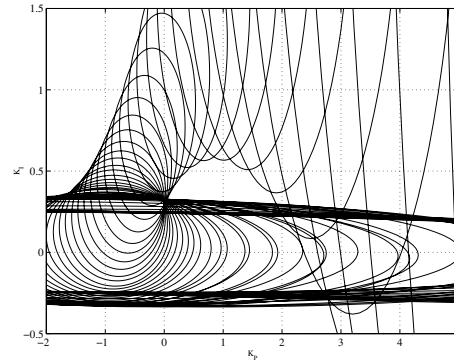Fig. 2.  $K_P, K_I$ plane , $w = \sin(\omega t)$



Fig. 3.  $K_P, K_I$ plane , $w = \sin(\omega t + \pi/2)$

The unfalsified regions are drawn with the transfer function of $V(z)$ that is discretized from $V(s)$ using zero-order holder. The falsified regions, the inside of the ellipses, are shown in Fig. 2 and Fig. 3. Fig. 2 is the result for $w = \sin(\omega t)$ and Fig. 3 for $w = \sin(\omega t + \pi/2)$. From these figures, we know that $w = \sin(\omega t + \pi/2)$ gives much better result. By the way, since $P$ is time-invariant in this problem, exact feasible region can be obtained by the frequency domain method of [10], and the unfalsified region of Fig. 3 is almost the same as the exact region.

Next, consider the reason. We will represent the equations in the continuous time domain, because we are usually more accustomed to the continuous time system than the discrete one. Since the falsification condition with $W = 0$ is represented as

$$\|Ve\|_2 < \gamma \|e + K_P y + K_I y_I\|_2 \tag{13}$$

, the difference is caused by the differences of the signals $e$, $y$, and $y_I$. Fig. 4 shows the response $y_I$ for the input $w = \sin(\omega t)$, and Fig. 5 for the input $w = \sin(\omega t + \pi/2)$. From these figures, we know that $y_I$ has a large bias for $w = \sin(\omega t)$, which makes the left-hand side of (13) large and brings about the failure of falsification. The effect of the phase shift on decreasing the bias is obvious from the Laplace transform. Namely, the Laplace transform of the integral of $w = \sin \omega t$ is

$$y_I = \frac{1}{s} \frac{\omega}{s^2 + \omega^2} = \frac{\omega}{s(s^2 + \omega^2)}$$

and it has a pole at $s = 0$, whereas that of $w = \sin(\omega t + \pi/2)$ is

$$y_I = \frac{1}{s} \frac{s}{s^2 + \omega^2} = \frac{1}{s^2 + \omega^2}$$

Therefore, we conclude that the integral element of $K(z)$ generates the bias for the sinusoidal input.

By the way, usually $V(s)$ has a pole close to the imaginary axis, $V e$ also tends to have a large bias for the same reason. This adds more unpredictable affect on the falsification condition.
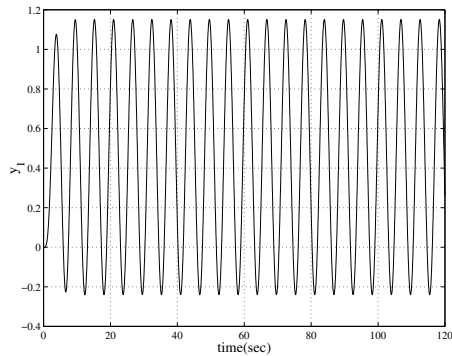


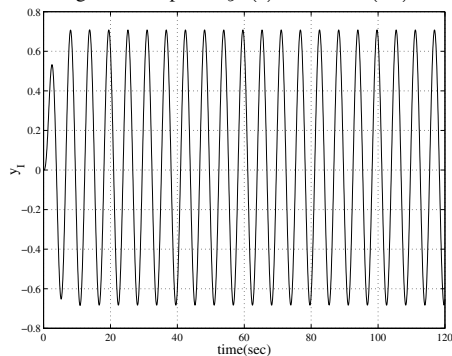Fig. 4.    Response $y_I(t)$ , $w = \sin(\omega t)$



Fig. 5.    Response $y_I(t)$ , $w = \sin(\omega t + \pi/2)$

**Remark 4 Stability region**    When the plant model can be linearized around the equilibrium point, we can easily draw all the set of PID gains that stabilize the linearized plant using the frequency response of the plant [10]. The stability region can be used for choosing proper regions from the unfalsified regions. For example, there are three vacant regions on the parameter plane in Fig. 3. Among the regions, the central region is the only region that satisfies

the stability condition. By drawing the stability set on the parameter plane, we can choose it appropriately from the unfalsified regions.

## III. APPLICATION TO STEERING TORQUE CONTROL

### A. Control problem

A steering torque control system is illustrated in Fig. 6. The control unit processes the signals from the steering angular sensor and steering torque sensor to output an adequate signal to the actuator so that a proper assist torque can be realized.

When the driver holds the steering wheel tight, the steering angle being given to the system is the external signal. The block diagram of the model is illustrated in Fig. 7, and we call this mode as **fixed control mode**. When the driver unlinks hands from the steering wheel or holds it light, the steering angle is affected by the steering system dynamics. The block diagram of the model is illustrated in Fig. 8 and we call this mode **free control mode**. These models are given in [12].
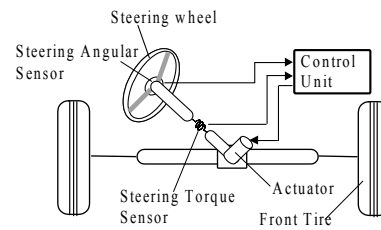


Fig. 6.    System overview of steering torque control

In these block diagrams, $\theta$, $u$, $y$, $r$ denote the steering angle, the control input, the steering torque, and the reference steering torque, respectively. The subsystem named 'target' is a highly nonlinear element that outputs the appropriate steering torque corresponding to the steering angle. The subsystem named 'plant' represents the dynamics of the steering system and the car body. The steering system is modeled as a two mass-damper 4th order system where each second order system has a friction feedback loop, and the car body dynamics is modeled as a second order linear time-invariant model. The subsystem named 'PID' denotes a PID controller to be designed.

The model is represented by using SIMULINK/ MAT-LAB. Therefore, the input output data of the system is easily obtained by simulation and they will be used for design directly. Note that detailed description of the plant model is not used in our design procedure. Our design problem is to find a PID controller which gives a good tracking performance for the two systems shown in Fig. 7 and Fig. 8 simultaneously.

### B. Design procedure

Let us draw unfalsified regions for the two models of the fixed and free control modes by using the falsification condition given in Theorem 1, and choose a PID controller

**7243**

from the intersection of the unfalsified regions. We will use the next PID controller

$$\tilde{K}(z) = K_P + \frac{K_I(0.001)}{z-1} + \frac{K_D(50z - 50)}{z - 0.9512} \qquad (14)$$

This is the $z$ transform of the next PID controller with the sampling period $\Delta T = 0.001 sec$ using zero-order holder.

$$\tilde{K}(s) = K_P + \frac{K_I}{s} + \frac{sK_D}{0.02s + 1} \qquad (15)$$

**Design procedure**

Step 1. In order to obtain the input output data $e, y$ in two modes, simulate two systems given in Fig. 9 and Fig. 10 for the next sinusoidal input with many frequencies

$$w = A\sin(\omega t + \pi/2) \qquad (16)$$

where the PID gain is fixed at some appropriate value $(K_{P_0}, K_{I_0}, K_{D_0})$. In the fixed control mode, since the steering angle is set to be zero, namely, $\theta = 0$, the responses $e, y$ are not affected by the subsystem 'target'.

Step 2. Choose $K_D$ some appropriate value (usually, $K_D = 0$).

Step 3. By using the measured data $e, y$, draw a falsified region on the $(K_P, K_I)$ plane for each frequency with $K_D$ fixed. Thus the unfalsified region is obtained on the $(K_P, K_I)$ plane. Choose $K_I$ from the region.

Step 4. Draw the falsified regions on the $(K_P, K_D)$ plane for each frequency with $K_I$ fixed at the value obtained in Step 3. Thus, the unfalsified region is obtained on the $(K_P, K_D)$ plane. Choose a PID gain from the unfalsified region.

Step 5. By iterating Step 3 and Step 4 with a severer $l_2$ performance index, we can make the the unfalsified region smaller. Stop this iteration if the unfalsified region becomes sufficiently small.
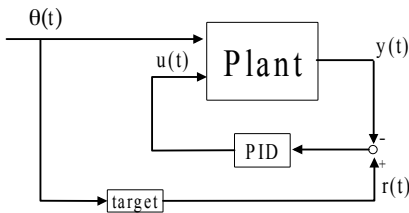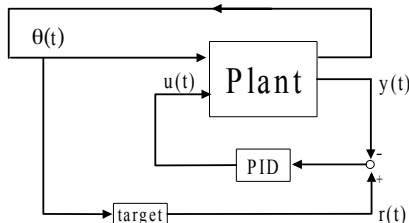


Fig. 7.   Fixed control mode model
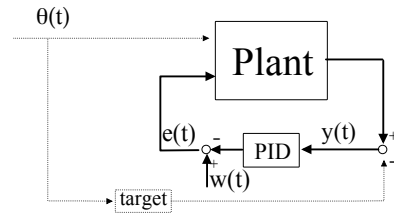


Fig. 8.   Free control mode model
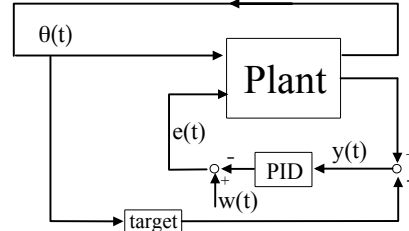


Fig. 9.   Fixed control mode model with $w(t)$



Fig. 10.   Free control mode model with $w(t)$

Simulation condition is as follows. The simulation interval is $T = 2(sec)$, and the sampling period is $\Delta T = 0.001(sec)$ for accurate simulation because of stiffness. PID gain is $K_{P_0} = 2.5, K_{I_0} = 0, K_{D_0} = 0$. The external signal is $w = 8\sin(\omega t + \pi/2)$ where the amplitude is determined so that the magnitude of $y(t)$ may cover the normal output range. The frequencies are the 200 points logarithmically equally spaced between $10^{-1} \sim 10^3(rad/sec)$.

We examine the following class of weighting functions where these are discretized using zero-order holder with the sampling period $0.001$ in the algorithm.

$$
\begin{aligned}
V(s) &= \frac{ps + 4}{2(ps) + 0.08} \\
W(s) &= \frac{(qs)^2 + 4(qs) + 4}{0.05(qs)^2 + 5(qs) + 50} \times 0.1
\end{aligned}
$$

We select the parameters $p$ and $q$ where the relation between the control performance and the sensitivity and complementary sensitivity functions of the linear time-invariant case is useful (for example, see [11]). As $p$ decreases from 0.18 to
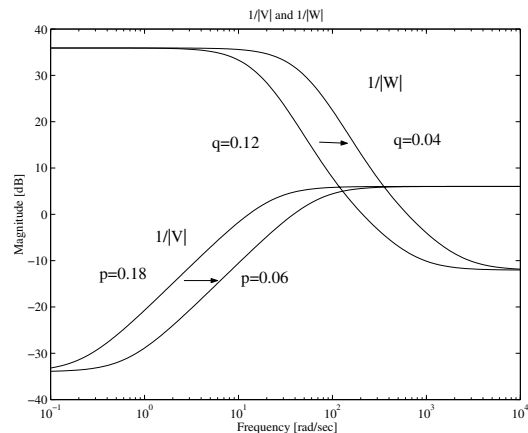


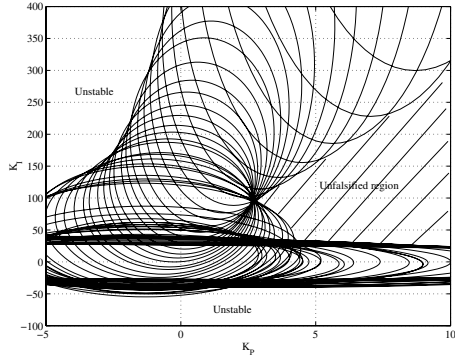Fig. 11.   The magnitude plots of $1/V$ and $1/W$

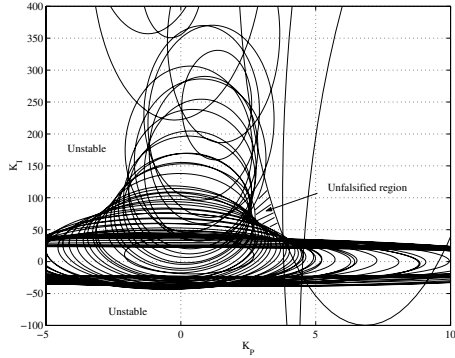Fig. 12.  $(K_P, K_I, 0)$  plane for fixed control mode



Fig. 13.  $(K_P, K_I, 0)$  plane for free control mode

0.06, the magnitude of $1/V$ moves to the right as shown in Fig. 11, and similarly, as $q$ decreases from 0.12 to 0.04, the magnitude of $1/W$ moves to the right.

We have chosen $p$ and $q$ so that unfalsified region exists. Especially, $W$ is mainly modified, because $1/|W|$ is the multiplicative uncertainty bound that can only be known by the experiment. After iterating the computation of the response and the region drawing, we have determined $p = 0.06$ and $q = 0.04$. By drawing the region for various weights, we were able to know how the uncertainty bound affects the unfalsified region.

First, falsified regions with $K_D = 0$ are drawn on the $(K_P, K_I)$ plane for the fixed control mode as shown in Fig. 12. The falsified regions are the inside of the ellipses, and three vacant regions can be seen in this figure. However, since the closed-loop system is not stabilized for a few sample gains of the left and lower vacant regions, we determine, partly based on our experience about the frequency domain method, that these regions may be falsified and that the right vacant region shown by the shaded portion is unfalsified. Of course, we may obtain the exact stability region following Remark 4 if necessary.

Falsified regions for the free control mode are drawn in Fig. 13. By superimposing these two figures, we find that the common unfalsified region exists in the vicinity of $K_P = 2.5 \sim 4.0, K_I = 70 \sim 120$. Therefore, we choose $K_I = 100$ in Step 3.

In Step 4, the falsified regions with $K_I = 100$ are drawn on the $(K_P, K_D)$ plane in Fig. 14 for the fixed control mode. Next, the unfalsified region is drawn in Fig. 15 for the free
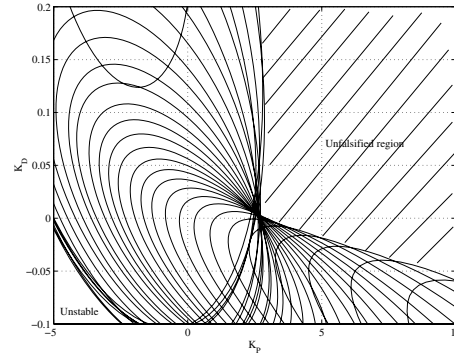


Fig. 14.  $(K_P, 100, K_D)$  plane for fixed control mode
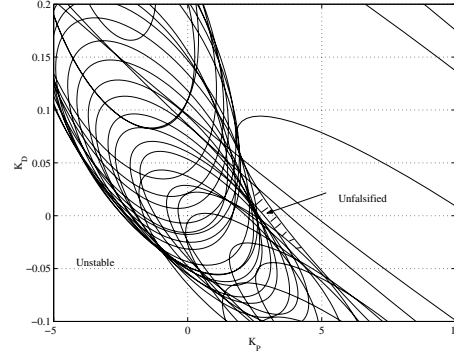


Fig. 15.  $(K_P, 100, K_D)$  plane for free control mode
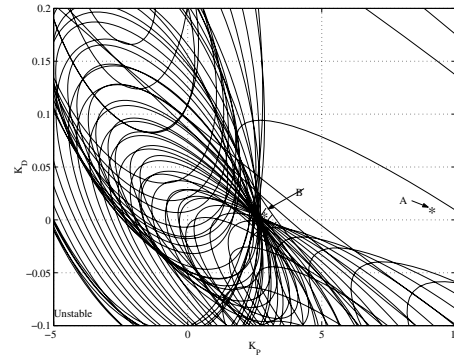


Fig. 16.  $(K_P, 100, K_D)$  plane for both modes

control mode. Superimposing Fig. 14 and Fig. 15 gives Fig. 16. From this figure, the common unfalsified region exists in the vicinity of $K_P = 2.8 \sim 4.0$, $K_D = -0.01 \sim 0.025$, $K_I = 100$.

### C. Evaluation of the result

We choose two controllers as shown by the points $A$ and $B$ in Fig. 16, and compare them by simulation. The controller $A : (K_P, K_D, K_I) = (9, 100, 0.01)$ lies in the falsified region of the free control mode and in the unfalsified region of the fixed control mode, and the controller $B : (K_P, K_D, K_I) = (3, 100, 0.01)$ lies in the unfalsified region of both modes. The results are shown in Fig. 17 - Fig. 20 where the dotted line shows the reference torque and the solid line shows the torque. In the fixed control mode, the torque tracks the reference well for both controllers. However, in the free control mode, the reference torque and the torque become oscillatory for the controller $A$. This is consistent with the previous result.
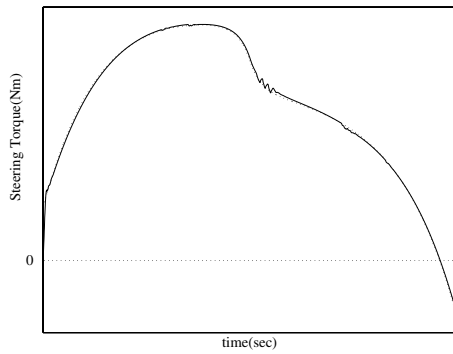
Fig. 17.   Evaluation of steering torque for controller A (fixed control mode)
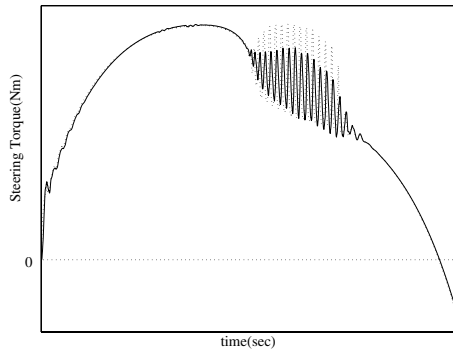


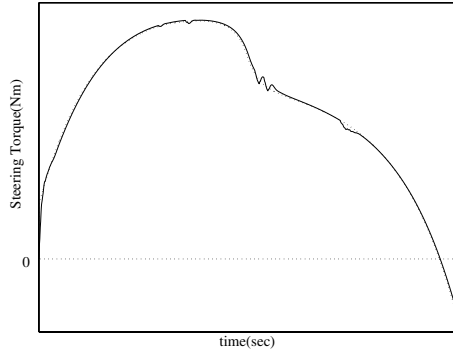Fig. 18.   Evaluation of steering torque for controller A (free control mode)



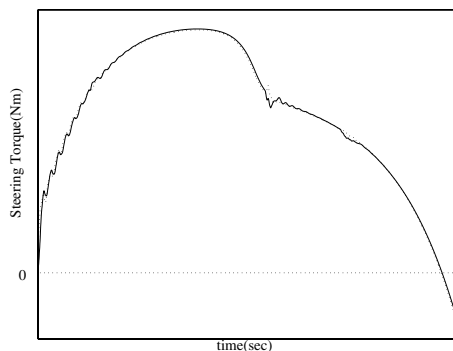Fig. 19.   Evaluation of steering torque for controller B (fixed control mode)



Fig. 20.   Evaluation of steering torque for controller B (free control mode)

## IV. CONCLUSION

In this paper, a simulation based controller design is demonstrated by applying our parameter space PID design method to the nonlinear dynamical model of a steering torque control system. The region of permissible PID gains on the parameter plane is obtained, which gives us useful information for tuning. Note that the unfalsified set in the 3 dimensional space is obtained by drawing the regions on the PI-plane for many fixed D gains.

One of the merits of our method is that if all the gains are falsified, we can conclude that no solution exist. This is because Theorem 1 is a necessary condition for the performance index and because no assumptions are made for the plant model. It shoud be noted that those design methods that are based on a sufficient condition often fail to find a solution even when a solution exists.

As a demerit, it is not guaranteed that most of the gains that should be falsified are falsified. Therefore, when the plant model can be linearized around the equilibrium point, it is recommended to apply the frequency domain method first in order to obtain the exact permissible region for the linearized model. Then, apply the proposed algorithm for the non-linear complex plant. By doing so, probably, we can know how the regions are deteriorated from the linearized case and we can determine the unfalsified sets more easily.

## REFERENCES

[1] J.C. Willems, Paradigms and puzzles in the theory of dynamical systems, *IEEE Trans. Automat. Contr.* , Vol.36 , No.3 , pp.259-294 , 1991.

[2] M.G. Safonov and T.C. Taso, The unfalsified control concept and learning, *IEEE Trans. Automat. Contr.* , Vol.AC-42 , No.6 , pp.843-847 , 1997.

[3] M. Jun and M.G. Safonov, Automatic PID tuning: An application of unfalsified control, *Proc. of the 1999 IEEE International Symposium on Computer Aided Control System Design*, pp. 328-333, 1999.

[4] T.C. Tsao and M.G. Safonov, Unfalsified direct adaptive control of a two-link robot arm, *International Journal of Adaptive Control and Signal Processing*, Vol. 15, pp. 319-334, 2001.

[5] F.B. Cabral and M.G. Safonov, Unfalsified model reference adaptive control using the ellipsoid algorithm, *Proc. of the 42nd Conference on Decision & Control*, pp. 3250-3255, 2003.

[6] E. G. Collins, Jr. and Y. Zhao, A Genetic Search Approach to Unfalsified PI Control Design for a Weigh Belt Feeder, *the International Journal of Adaptive Control and Signal Processing*, Vol. 15, pp. 519-534, 2001.

[7] B.R. Woodley, J.P. How, and R.L. Kosut, Direct unfalsified controller design - Solution via convex optimization, *Proc. of the American Control Conference*, pp. 3302-3306, 1999.

[8] M.Saeki, Unfalsified control approach to parameter space design of PID controllers, *Trans. of the Society of Instrument and Control Engineers*, Vol. 40, No. 4, pp. 398-404, 2004.

[9] M.Saeki, A. Takahashi, O. Hamada, and N. Wada, Unfalsified parameter space design of PID controllers for nonlinear plants, *IEEE Conference on Control Applications*, pp. 1521-1526, 2004.

[10] M. Saeki and J. Kimura, Design method of robust PID controller and CAD system, *11th IFAC Symposium on System Identification*, Vol. 3, pp. 1587-1593, 1997.

[11] J.C. Doyle, B.A. Francis, and A.R. Tannenbaum, *Feedback Control Theory*, Macmillan Publishing Company, 1992.

[12] Masato Abe, *Vehicle Dynamics and Control*, Sankaido Publishing Co.,LTD., Ch. 5, 1994 (in Japanese).